# Crystallization by selective evaporation using membrane pervaporation: Application to l-glutamic acid to control polymorphism

Maya Khellaf, Xiaoqian Huang, Jean-Pierre Valour, Denis Mangin, Catherine Charcosset, Elodie Chabanon

# Crystallization by selective evaporation using membrane pervaporation: Application to L-glutamic acid to control polymorphism

**Maya KHELLAF, Xiaoqian HUANG, Jean-Pierre VALOUR, Denis MANGIN, Catherine CHARCOSSET, Elodie CHABANON***

Univ Lyon, Université Claude Bernard Lyon 1, CNRS, LAGEPP UMR 5007, 43 boulevard du 11 Novembre 1918, F-69100, VILLEURBANNE, France

*Article submitted to the*

*Journal of Membrane Science – August 2022*

*: Corresponding author

☎: +33 4 72 43 18 52

Email: elodie.chabanon@univ-lyon1.fr

## ABSTRACT

Crystallization is an important unit operation in process industries, driven by supersaturation, i.e. the solute concentration difference between solution and equilibrium. Hence, to finely control the product qualities, controlling mass and/or heat transfer is crucial. Membrane pervaporation, based on a selective evaporation technique, appears as a process able to limit phase transition and control polymorphism. In this work, a semi-continuous system is developed for the crystallization of L-glutamic acid, which has two polymorphic forms. Hydrophilic HybSi® membranes are chosen. The influence of different operating parameters on process performance in terms of solvent separation, solute crystallization and control of polymorphism is investigated. Results validate the proof of concept and highlight the preferential crystallization of a polymorphic form over the other. Hence, the $\alpha$-form is usually favoured except when the $\beta$-form is seeded, or at high temperature. Temperature appears as the parameter influencing mostly the membrane selectivity and the polymorph generated. However, concentration polarization and fouling, due to the deposit of L-glutamic acid crystals on the membrane surface, are reported and decrease the process performance. Both phenomena are caused by a high local supersaturation close to the membrane surface in addition to a local cooling due to the water evaporation during pervaporation.



## KEYWORDS

Pervaporation, membrane crystallization process, HybSi® membrane, polymorphism control, L-glutamic acid


## 1. INTRODUCTION

Crystallization is one of the most important unit operations used to produce, purify or separate solid products. The pharmaceutical industry is a major area of application for crystallization as about 90% of pharmaceuticals contain active ingredients in the crystalline form [1,2]. The ordered structure of crystals facilitates the rejection of impurities, making purification steps energy-efficient and cost-effective. However, the compounds to be crystallized may adopt a different structural conformation of the crystal lattice while being molecularly identical. This phenomenon is known as polymorphism. Two polymorphic forms have different physical, mechanical and thermal properties (melting point, density, compressibility, shape, solubility, dissolution rate, friability, purity...). These differences can have a significant influence on the stability and bioavailability of the active ingredient, but also the processing capability of the product in downstream processes (filtration, drying and processing). Due to the therapeutic objectives of the manufactured products, the control of the crystallization process is crucial in the pharmaceutical industry as a separation process of intermediates and as a final step in the production of active ingredients. Batch crystallization in stirred reactors is the oldest approach and remains the predominant method today [3]. Despite its robustness, it has some limitations such as heterogeneities at the micro-mixing scale affecting the repeatability of the production, the homogeneity of the final product from batch to batch and even the polymorphic phase crystallized [4]. For this purpose, membrane processes have been recently proposed as an alternative to improve crystallization performance. They are often studied as tools for intensifying conventional processes because they offer a good selectivity, large surface area per unit of volume, and the ability to control contact and/or mixing between two phases [5]. Applied to crystallization, membrane processes would allow the control of nucleation and growth kinetics, fast crystallization rates, good control of supersaturation levels and polymorphism [6,7]. According to several pioneering studies, membrane processes appear to be a tool to achieve these goals [8–10]. Di Profio et al. were among the first to

publish studies on the crystallization of active ingredients by membrane processes. In particular, they studied the case of polymorphic forms of glycine [11,12], paracetamol [8,11,13] and carbamazepine [13,14] by developing membrane crystallizers where the porous membrane matrix acts as a selective barrier for solvent evaporation, modulating the final degree and rate of supersaturation generation.

Among the membrane processes of growing interest, pervaporation is chosen in this study as an innovative process for crystallization. Pervaporation is generally used for separating a liquid mixture by selective transfer through a dense membrane, where the constituents permeate and undergo a change of state by vaporizing [15]. In the pharmaceutical field, it is mainly used for effluent dehydration, solvent recovery and water removal during reactions [16–20]. As far as crystallization is concerned, this technique remains relatively unexplored, despite the industrial potential of an intensified process. Indeed, crystallization using membrane pervaporation would allow a better control of the mass transfer, through the selective evaporation of the solvent thus providing the supersaturation necessary to drive crystallization [7]. Several studies are being conducted to develop new membrane materials applicable to pervaporation for the improvement of separation properties of organic or hydro-organic mixtures [21,22]. However, only a few studies have reported the use of pervaporation for the crystallization of organic compounds. The first mentioning the combination of these two processes dates back more than a century ago when Kober reported the pervaporation phenomenon through a dense membrane and introduced the percrystallization process [23]. It was only years later that Böddeker et al. [24] studied the sorption and pervaporation of vanillin from aqueous solution. In another study by Zhang et al. and later by Li et al. [25,26], high-purity phenol crystals (99.8%) were recovered from a dilute aqueous solution. These authors developed a two-stage condenser system to collect the permeate containing phenol crystals using PEBAX membranes [25]. More recently, Zeng et al. [27] developed a two-step operation where pervaporation for water removal is first conducted using NaA zeolite membrane, followed by a cooling crystallization and filtration to collect sodium pyruvate and ethanol. However, performance limitations related to the use of membrane technologies for crystallization have been reported in the literature. One of the major obstacles is the problem of membrane fouling. This results in a decrease of membrane permeability due to the deposition of suspended or dissolved components on the membrane surface [28]. Several studies in the literature reported the influence of operating parameters on fouling. Indeed, Kieffer et al. have shown that, for their experimental conditions, an increase in the inner diameter of the hollow fibers was sufficient to reduce fouling, but no long-term experiments have been conducted [29]. Much research has been carried out on membrane pre-treatment to limit fouling, based on the assumption that wetting the membrane surface would avoid fouling effects [28,30–33]. Other researches have been carried out on the use of cleaning solutions or additives to overcome fouling [34–37], but by these means, it is more difficult to maintain the initial performance of the process and it may also require the use of aggressive chemicals. Another phenomenon can lead to a significant decrease in transmembrane flux : concentration polarization [38–40]. It corresponds to the formation of a boundary layer of polar molecules on the membrane surface. The impact of concentration polarization is specific to each separation process. The main factor influencing this phenomenon is the hydrodynamics of the process. Indeed, increasing the flow velocity or using turbulence promoters upstream of the membrane are technical means to decrease the thickness of the boundary layer.

This work aims to determine the operating parameters of the pervaporation process controlling the final properties of the product to be crystallized (crystal size and polymorphic form) and to identify the limiting parameters of the process. To achieve the objectives of this study, a semi-continuous experimental setup has been developed. L-glutamic acid is chosen as a model compound as it

crystallizes under two well-known monotropic polymorphs: the stable β-polymorph (needle-like shape) and the metastable α-polymorph (prismatic shape). The experimental results of this study have highlighted the possibility of controlling the polymorphic form but also the limiting points of the process operation.

# 2. MATERIALS & METHODS

## *2.1. Membranes and module*

Organic/inorganic hybrid membranes HybSi® are used in this work. The HybSi® membrane is a hybrid ceramic membrane [41–43] with a so-called "sandwich-like" structure (cf. Figure 1): i.e. a ceramic-based substrate successively covered by an amorphous silica layer and a thin selective layer of HybSi® in which silane precursors, such as BTESE (bis(triethoxysilyl)ethane) or BTESM (bis(triethoxysilyl)methane) are incorporated [41,44].

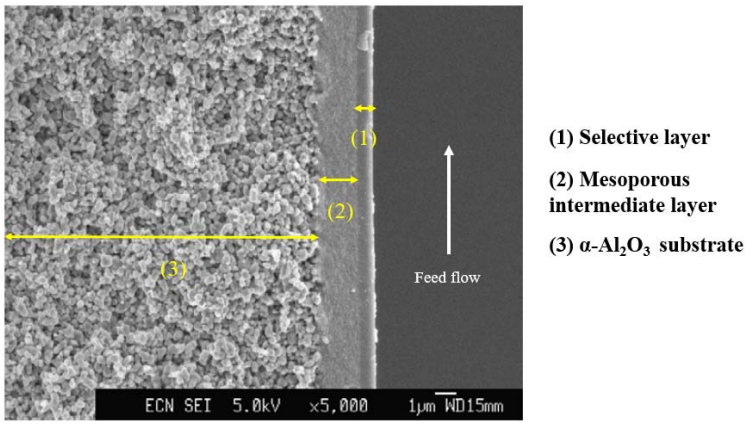


***Figure 1.*** *Cross-sectional SEM picture of HybSi® membrane [43]*

For the following experiments, three tubular HybSi® membranes, purchased from Orelis Environment (Alsys Group, France), are used. The membranes are from the same production batch and correspond to the standard J05-A-X range with BTESM precursor. They are referred to M1, M2 and M3. The membranes are monotubular with an internal diameter of 6mm, an external diameter of 10mm, a length of 25cm and an effective area of 47cm$^2$.

## *2.2. Experimental setup*

The experimental setup developed is shown in Figure 2.

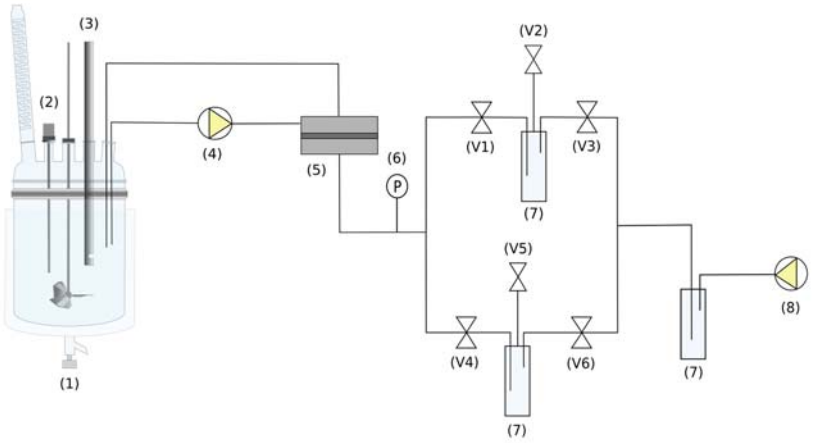


***Figure 2.*** *Experimental setup for the crystallization pervaporation unit. (1) Double jacketed 1L reactor; (2) Temperature probe; (3) EZ video probe; (4) Peristaltic pump; (5) Membrane module; (6) Pressure gauge; (7) Vacuum traps immersed in liquid nitrogen; (8) Vacuum pump; (V1-6) 2-way valves.*

The feed mixture is put in a 1L double-jacketed reactor. The reactor temperature is controlled by a thermostatic bath (Ministat 230 Pilot One, Huber, Germany) equipped with a Pt100 temperature sensor. A 3-blade mixel TT® stainless steel propeller with a fixed speed of 400rpm provides stirring. The feed solution flows through a 10mm internal diameter polyvinyl chloride (PVC) tubing using a peristaltic pump (603S, Watson Marlow, UK) to the membrane module. The feed solution, at atmospheric pressure, flows on the lumen side of the tubular membrane. The retentate, i.e. the supersaturated solution after the selective evaporation of water, is reintroduced into the reactor. The permeate side is under vacuum allowing the selective transfer of water under vapour from the feed solution. The vacuum pressure, between 3 and 8mbar, is regulated by a PID controller and a Pirani capacitive gauge (0-100mbar, CMR362, Pfeiffer Vacuum, Germany) connected to a control unit (RVC 300, Pfeiffer Vacuum, Germany). The vacuum pump is a vane pump (Adixen Pascal 2005SD, Pfeiffer Vacuum, Germany) with a nominal flow rate of 5.4$m^3$/h and a total pressure limit closed (open) air ballast of $2.10^{-3}$mbar ($10^{-2}$mbar). The permeate is then condensed in vacuum traps, immersed in liquid nitrogen, and regularly recovered during the experiment.

Hence, two vacuum traps are placed in parallel and operated alternately. A set of valves is used to switch between the two traps (cf. Figure 2). Finally, a safety trap, connected in series and operating continuously, is installed to protect the vacuum pump and to recover and quantify the permeate that is not condensed in the first trap.

### *2.3. Chemical products*

For all experiments, the following products are used:

- Ultrapure water (Millipore Synergy® purification system, resistivity = 1.2mΩ.cm);
- Anhydrous absolute ethanol (Carlo Erba Reagent S.A.S, chemical purity≥ 99.9%);
- β-polymorph of L-glu corresponding to the commercial product (Sigma Aldrich Co. Ltd, purity ≥ 99.5%);
- α-metastable form obtained according to the protocol previously described [45].

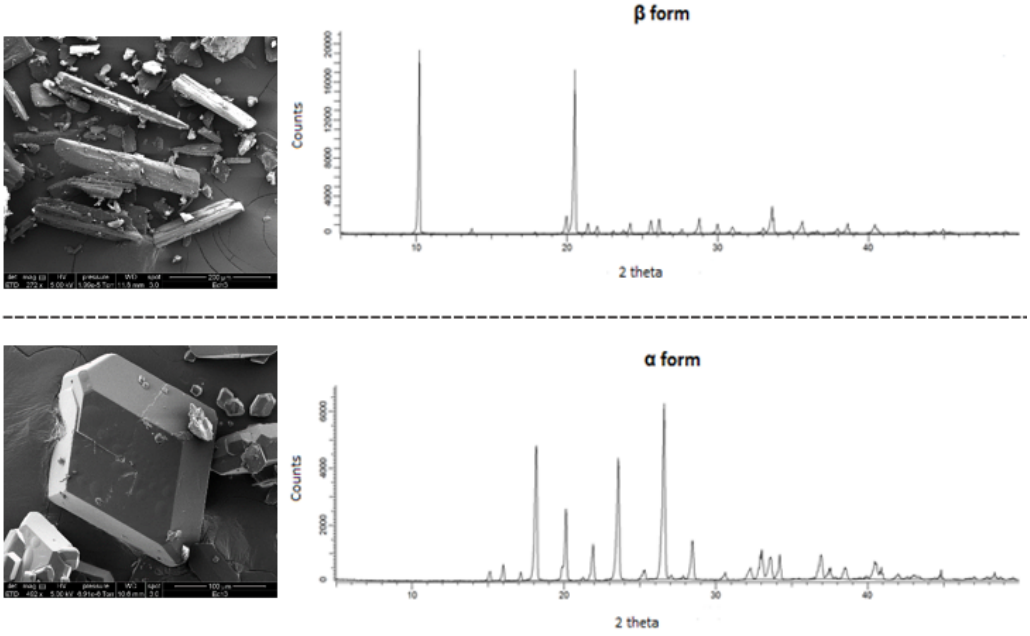


***Figure 3.*** *SEM micrographs and XRD patterns of the stable β-form and the metastable α-form of L-glutamic acid*

Figure 3 presents the SEM micrographs and XRD patterns of both polymorphs. It is worth noting that, as expected, the α-form is prismatic while the β-form is needle-like. The XRD patterns show the presence of only one polymorph in each case with characteristic peaks at 10.2° 2 theta for the β-form and at 18.1° 2 theta for the α-form.

### *2.4. Operating conditions and protocol*

A 1L of water/ethanol solution previously prepared by weighing (PM6000, Mettler Toledo, Germany) is introduced into the reactor. Three initial ethanol mass fractions ($w_{EtOH,ini}$) are investigated: 0.122, 0.252 and 0.344. A precise amount of commercial L-glu is weighted and added to the solution. The amount of L-glu is calculated from the solubility data determined in a previous study [45], for an initial supersaturation fixed at 1.4 (cf. Table 1).

***Table 1.*** *Mass of L-glutamic acid added to the reactor according to the temperature and the composition*

| $w_{EtOH,ini}$ (-) | at 25°C | | at 40°C | |
|---|---|---|---|---|
| | Solubility (g/kg of solution) | Mass added to the reactor (g) | Solubility (g/kg of solution) | Mass added to the reactor (g) |
| 0.122 | 4.989 | 6.818 | 8.451 | 11.600 |
| 0.252 | 2.815 | 3.707 | 5.408 | 7.148 |
| 0.344 | 1.920 | 2.469 | 3.794 | 4.892 |

First, L-glu crystals are dissolved at a temperature of 20°C above the working temperature for about 1h. The video probe immersed in the reactor monitors the dissolution of the crystals. The solution is then cooled to the working temperature. At the same time, the peristaltic pump is switched on at a fixed flow rate ($Q_v$ = 135L/h, i.e. Re > 7000) to wet the membrane at the desired temperature for at least 45min before starting pervaporation. This is the time required to reach equilibrium between the membrane and the feed solution [46]. When the reactor temperature is stable, two samples of the

solution are taken, one is analysed using NMR to determine the initial ethanol mass fraction, and the other is introduced into an oven at 85°C for 24h to determine the initial L-glu concentration of the solution.

Then, the vacuum pump is switched on when the above conditions are set. Valves V1 and V3 are opened and the experiment begins. Valves V2, V4, V5 and V6 remain closed (cf. Figure 2). Trap changes are made every hour. The frequency of trap changes is optimised to avoid the risk of clogging.

Vacuum pressure and temperature are monitored every minute for the first 5min and then every 15min. At each trap change, a sample of the retentate is taken and analysed. The recovered trap is warmed to room temperature to recover the frozen permeate. Once in a liquid state, the trap is returned to atmospheric pressure through the V2 valve before being removed from the setup. The permeate is then introduced into a glass vial and hermetically sealed. Vials are weighed before and after on an analytical balance (± 0.001g, PM200, Mettler Toledo, Germany).

About 2mL of retentate is taken every 2h for analysis. A video is recorded before each trap change to follow the appearance and growth of crystals in the reactor.

The experiments are carried out for 8h in order to follow the evolution and growth of the crystal and any phase transitions.

At the end of the experiment, the L-glu suspension is removed. A heated ultrapure water solution is added to the reactor and flows through the system. The membrane, the reactor and all the system including the peristaltic pump and the tubes are cleaned with the heated water to dissolve and remove L-glu residues. Lastly, the membrane, the reactor and all the system are washed with clean water several times and dried at ambient temperature. To check the membrane regeneration, pervaporation is carried out with a water/ethanol solution.

Several parameters are measured during the experiments. The total flux of permeate is determined according to:

$$J_{tot} = \frac{m_p}{S\,t} \qquad \textbf{Eq.1}$$

Where $J_{tot}$ is the total flux of permeate (kg/(m$^2$.h)), $m_p$ is the mass of permeate recovered in the trap (g) for a period of time t (h) and S is the effective membrane area (m$^2$).

The permeate samples are then analysed by NMR to determine the mass fraction of ethanol and the partial fluxes from the following equation:

$$J_i = J_{tot} \cdot w_i^p \qquad \textbf{Eq.2}$$

With $J_i$ the partial flux of compound i (water or ethanol) (kg/(m$^2$.h)) and $w_i^p$ the mass fraction of compound i (water or ethanol) in the permeate (-).

The separation factor, which quantitatively describes the quality of the separation, is defined by:

$$\beta_{water/EtOH} = \frac{w_{water}^p / w_{EtOH}^p}{w_{water}^f / w_{EtOH}^f} \qquad \textbf{Eq.3}$$

Where $w_{water}^p$ and $w_{EtOH}^p$ are the mass fractions respectively of water and ethanol in the permeate (-) and $w_{water}^f$ and $w_{EtOH}^f$ in the feed solution (-).

The supersaturation factor, which describes the deviation of the L-glu concentration, noted C (in $g.L^{-1}$), from its solubility, noted C* (in $g.L^{-1}$) is estimated by:

$$\beta = \frac{C}{C^*} \quad \textbf{Eq.4}$$

## *2.5. Characterization methods*

### *2.5.1. In situ* observation with the EZ video probe

A video probe (EZProbe® 12005) is immersed in the stirred suspension and allows real-time monitoring: before the experiment, to check the complete dissolution of crystals and during the experiment to observe the apparition of crystals, growth and agglomeration. The video probe has a field size of 720µm × 540µm and allows acquiring 25 frames per second [47].

### 2.5.2. Optical microscopy (OM)

After drying at room temperature for at least 24h, the crystals are observed under optical microscopy (OM) to identify the polymorphic phases obtained and to evaluate, at the same magnification, crystals' size. The optical microscope used is a Leica DM2000 LED, with different objectives with magnification of 5x, 10x, 20x, 40x and 100x. The microscope is equipped with a digital camera connected to a computer, which allows high-resolution image acquisition using the Leica Application Suite (LAS) software.

### 2.5.3. X-ray diffraction (XRD)

XRD analyses are carried out to determine the predominant polymorph formed. The device used is a Bruker D8 Advance diffractometer operating at room temperature with Kα radiation of wavelength 1.54060Å, a tube voltage of 40kV and a current of 40mA. Diffraction patterns are recorded using a step scan method at 2 Theta values between 5° and 50° with a step size of 0.02°. Before analysis, the crystals are deposited on flat-bottomed neutral supports. The diagrams obtained are then processed using the DIFFRAC.EVA software and the results obtained are compared with the database to identify the polymorphic phases.

### 2.5.4. NMR analysis

The quantification of ethanol in the permeate is determined by NMR. This method of analysis has the advantage of not being limited by the composition. The analyses are performed with a BRUKER 400MHz NMR spectrometer at room temperature (298 K) with a BBFO probe for 5mm NMR tubes.

Ethanol shows two characteristic signals: a triplet signal at 1.19ppm, corresponding to the protons of the methyl group, $CH_3$-, and a multiplet signal at 3.66ppm for the protons of the methylene group, -$CH_2$-. Sodium 3-trimethylsilyl-3,3,2,2-tetradeuteriopropionate (STP) is chosen as the internal standard because it is soluble in water and available at high purity. It has a simple 1H NMR spectrum consisting of a single singlet of 9 protons that never overlaps with an ethanol signal [48]. The spectra are all referenced to the TSP singlet peak at 0.0ppm. Samples are prepared as follows: 10mg of STP (98 atom %D, Sigma-Aldrich, USA) is dissolved in 400µL of $D_2O$ (99.9 atom %D, Sigma-Aldrich, Canada) to which 300µL of the sample to be analysed is then added. The NMR spectra obtained are processed using BRUKER's TopSpin 4.1.0 software. To obtain reliable results, phasing and baseline correction over the entire spectral range are performed manually.

# 3. RESULTS

## *3.1. Membranes ageing*

Before starting crystallization experiments, pervaporation with water/ethanol solution is performed to measure the separation factor and the total permeate flux of the original membranes. The separation factor and the permeate flux (cf. Table 2) are determined at 25°C, with a permeate pressure of 3mbar and an initial ethanol mass fraction of 0.122 in the solution. Both parameters are almost constant during the experiments of 5h (data not shown). The values indicated in Table 2 are thus average values measured on 5h. The separation factor and the total flux for the three membranes M1, M2 and M3 are similar, in the range of 3.6 - 4.3 and 2,300 - 2,500g/(m².h), respectively.

***Table 2.*** *References and characteristics of the membranes used*

| Membrane | Membrane reference | Separation factor $\beta_{water/EtOH}$ (-) | Total flux (g/(m².h)) |
|---|---|---|---|
| **M1** | J05-A-10 | 3.69 | 2,480 |
| **M2** | J05-A-09 | 3.61 | 2,447 |
| **M3** | J05-A-07 | 4.34 | 2,293 |

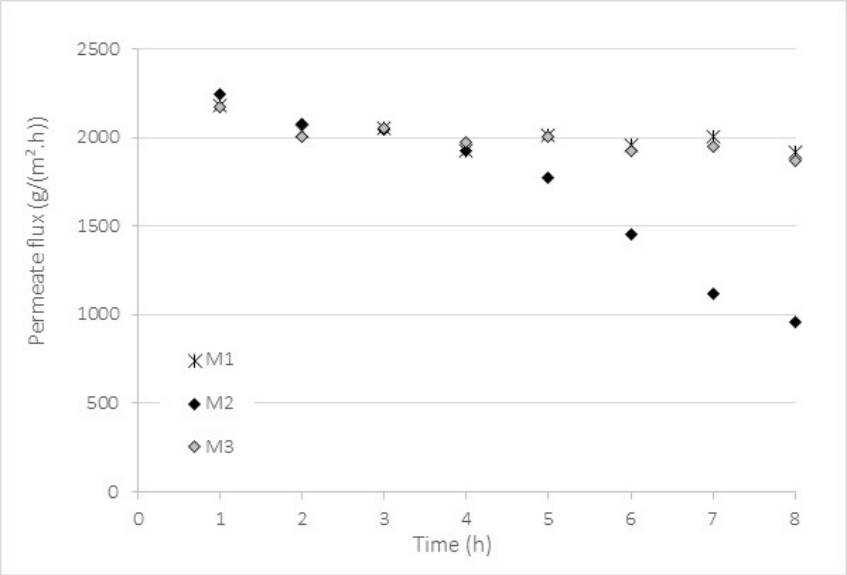


***Figure 4.*** *Permeate flux variation with time for "new" membranes, $w_{EtOH,ini}$ = 0.252, T = 25°C and $P_{permeate}$ = 3mbar*

The performance of M1, M2 and M3 membranes are investigated with the "new" membranes, i.e. for their first use with L-glu. Experiments are carried out under the same operating conditions: $w_{EtOH,ini}$ = 0.252, T = 25°C and $P_{permeate}$ = 3mbar. Results are reported in Figure 4 and show that the permeate fluxes have the same evolution during the first 4h of experiment. The initial flux is close to 2,200g/(m².h) for the three membranes and decreases after 2h, reaching 2,039g/(m².h) for M1, 2,075g/(m².h) for M2 and 2,006g/(m².h) for M3. The permeate flux then remains relatively stable for M1 and M3 after 8h. However, a significant decrease is observed for M2 after 4h of experiment, from 1,923g/(m².h) to 960g/(m².h). The flux decrease can be explained by different phenomena, in

particular concentration polarization and/or membrane fouling. These phenomena appear more or less rapidly for the same experimental conditions. The small variation of the flux, as the one observed with M1 and M3, is only obtained during the first use of the membranes.

Table 3 highlights that the same polymorphic form is obtained for the three membranes: the $\alpha$-form. Thus, the decrease in flux over time (observed for M2) does not influence the crystallization of one polymorph over another.

**Table 3.** Polymorphic forms obtained after 8h with "new" membranes

| **Membrane** | **M1** | **M2** | **M3** |
|---|---|---|---|
| **OM Picture (enlargement x 5)*** | 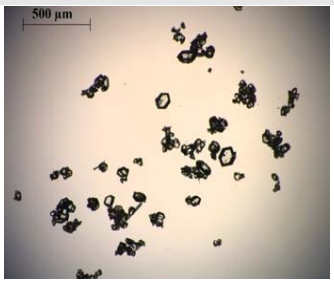  |   | 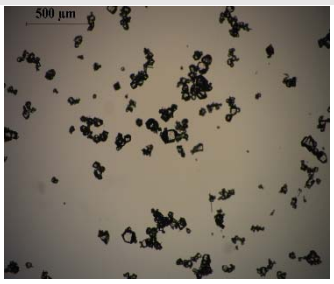  |
| **Polymorphic form obtained** | Mainly α | Mainly α | Mainly α |

**OM pictures have the same scale: 500µm*

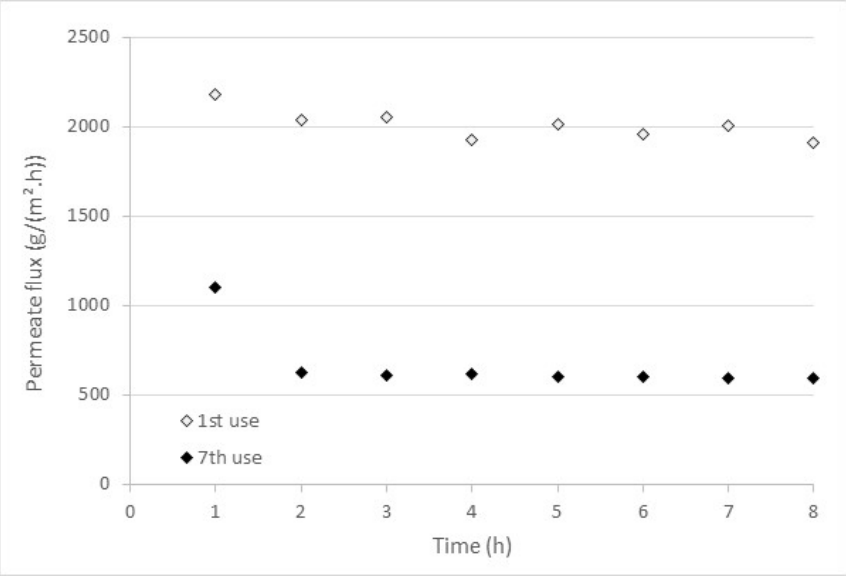


***Figure 5.*** *Permeate fluxes as a function of time for several uses of M1 membrane, $w_{EtOH,ini}$ = 0.252, T=25°C and $P_{permeate}$ = 3mbar*

However, the membrane performance decreases after several uses (cf. Figure 5), despite regular regeneration of the membrane. Figure 5 shows the fluxes evolution obtained after several uses for the M1 membrane, i.e. the 1st use and the 7th use. The initial flux decreases from 2,181g/(m².h) to 1,100g/(m².h) between the 1st and the 7th use. The fluxes stabilize at around 2,000g/(m².h) and 600g/(m².h) after 8h, during the 1st and the 7th use, respectively. The fluxes are thus divided by 3 between the 1st and the 7th use.

These results suggest membrane fouling, concentration polarization and/or surface modification of the HybSi® membranes [43,49] (by adsorption of L-glu molecules at the membrane surface and/or degradation of the selective surface by L-glu crystals). These phenomena are discussed in a following section.

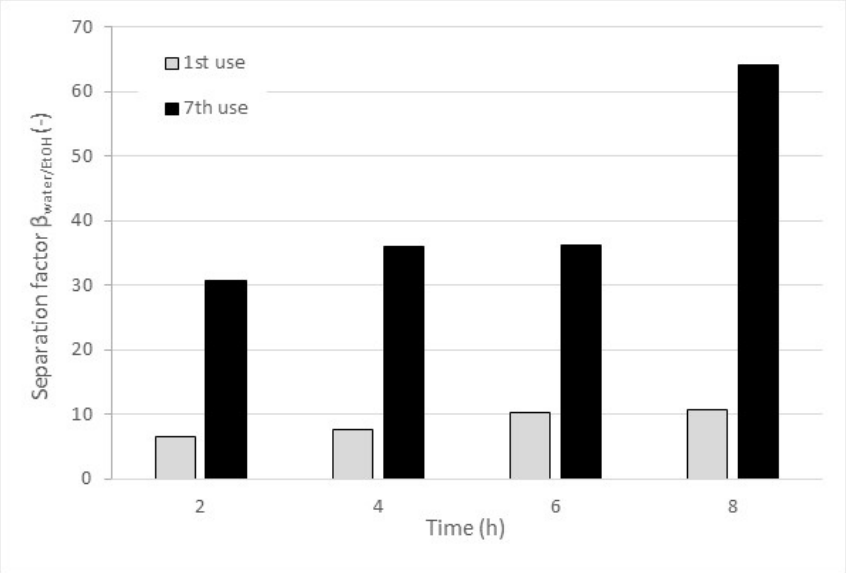


***Figure 6.*** *Separation factors as a function of time for the M1 membrane after the 1st use and 7th use, $w_{EtOH,ini}$ = 0.252, T=25°C and $P_{permeate}$ = 3mbar*

Simultaneously with the decrease in total flux over time, a decrease in ethanol flux is observed increasing thus the water/ethanol separation factor (cf. Figure 6). After 7 uses, the membrane still maintains a high selectivity towards the water. This result is consistently observed in all subsequent experiments. Thus, although the permeate flux decreases with time, the membrane performance in terms of water/ethanol separation increases.

***Table 4.*** *Polymorphic forms mainly obtained after 1st and 7th use, M1 membrane, $w_{EtOH,ini}$ = 0.252, T=25°C and $P_{permeate}$ = 3mbar*

| **Number of use** | **1st use** | **7th use** |
|---|---|---|
| **Mean flux (g/(m².h))** | 2,011 | 669 |
| **OM Picture (enlargement x 10)*** | 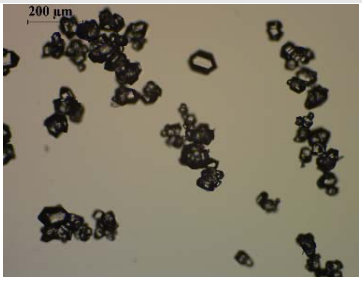  | 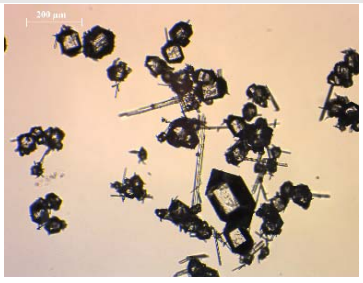 |
| **Polymorphic form obtained** | Mainly α | Mainly α (β crystals observed by the video probe but unquantified in XRD) |

**OM pictures have the same scale: 200µm*

Table 4 shows that the same polymorphic form is obtained, despite the decrease of the mean flux during the experiment, as confirmed by the pictures taken at the end of the 1st and the 7th experiment. Hence, the polymorphic form seems to depend more on the operating conditions (initial composition of the liquid phase, temperature) than on the permeate flux. However, β crystals are also observed with OM after the 7th use but the amount is too small to be detected by XRD, i.e. lower than 1%wt.

### *3.2. Temperature influence*

In pervaporation, the permeate flux strongly depends on the temperature. Thus, two temperatures, 25°C and 40°C, are investigated for $w_{EtOH,ini}$ = 0.122 and $P_{permeate}$ = 8mbar. The results obtained are reported in Figure 7.

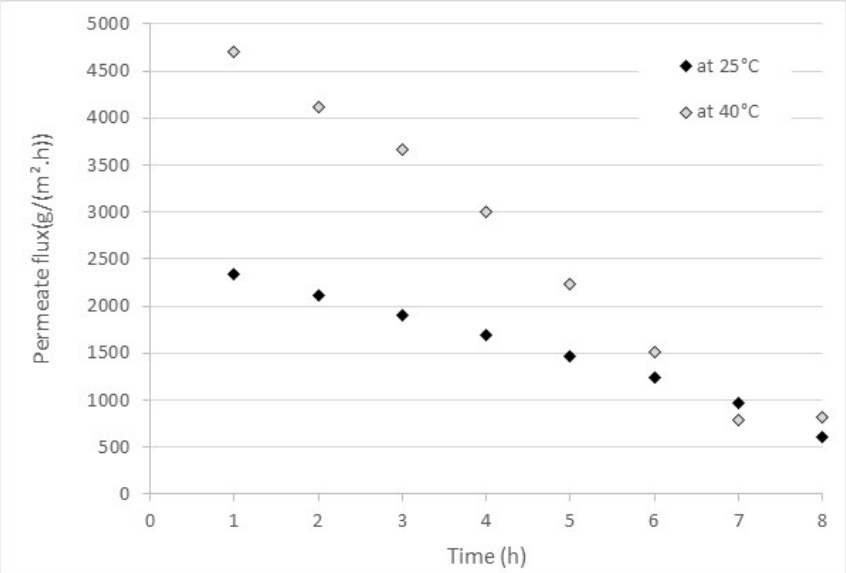


***Figure 7.*** *Total permeate flux as a function of time, $w_{EtOH,ini}$ = 0.122 and $P_{permeate}$ = 8mbar*

The increase in temperature has a beneficial effect. Indeed, it leads to an increase of the initial permeate flux, from 2,347g/(m².h) to 4,703g/(m².h). This result is consistent with what is observed for pervaporation alone where the permeate flux increases with rising temperature [43,46,50].
However, the decrease in permeate flux is more pronounced at 40°C than at 25°C. Furthermore, after 7h, the permeate fluxes reach similar values, around 900g/(m².h). This result suggests that a higher permeate flux (as obtained at 40°C) leads to a higher concentration polarization and/or fouling of the membrane. This phenomenon will be discussed in a following section.

***Table 5.*** *Polymorphic forms obtained at 25°C and 40°C, $w_{EtOH,ini}$ = 0.122 and $P_{permeate}$ = 8mbar*

| **Temperature** | **25°C** | **40°C** |
|---|---|---|
| **Membrane (number of use)** | M2 (3rd use) | M2 (5th use) |
| **Mean Flux (g/(m².h))** | 1,675 | 2,606 |
| **OM Picture (enlargement x 5)*** | 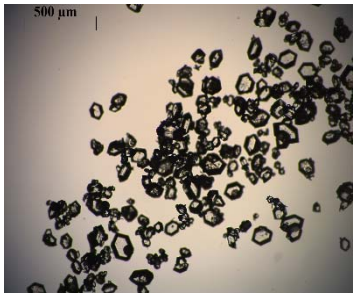  | 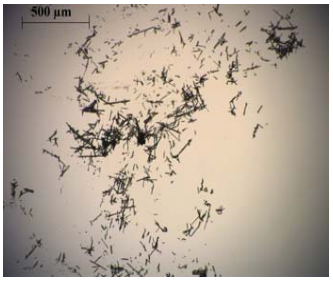  |
| **Polymorphic form obtained** | Mainly α | Mainly β |

**OM pictures have the same scale: 500µm*

The temperature increase induces a significant rise of the mean flux (over 8h of experiment), from 1,675g/(m$^2$.h) at 25°C to 2,606g/(m$^2$.h) at 40°C (cf. Table 5).Moreover, results highlight that at 25°C, the α-form is the main polymorphic form detected. While, the β-form is the main polymorphic form at 40°C. These observations made *in situ* by the video probe are also confirmed by OM pictures and by XRD analysis. Hence, the temperature allows producing selectively one of the polymorphic form for $w_{EtOH,ini}$ = 0.122.

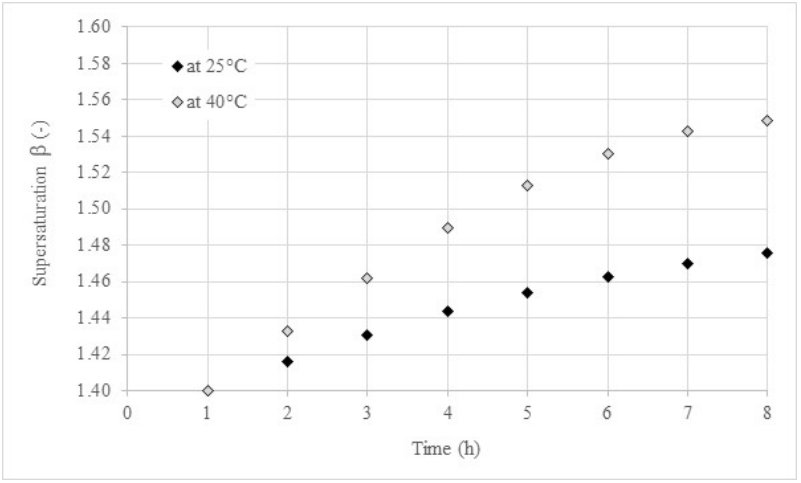


***Figure 8.*** *Supersaturation as function of time at the operating temperature of 25°C and 40°C, $w_{EtOH,ini}$ = 0.122 and $P_{permeate}$ = 8mbar*

Figure 8 reports the evolution of the supersaturation in the reactor during the experiment. Results show that the increase of the supersaturation with time is higher at 40°C than at 25°C, which is consistent with flux results reported in Figure 7. At this step, it seems that either the temperature or the supersaturation variation during the experiment is able to control polymorphism.

### *3.3. Influence of the initial ethanol mass fraction*

Three mass fractions of ethanol in the initial water/ethanol mixture are studied to evaluate the influence of this parameter on the permeate flux and crystal production: 0.122, 0.252 and 0.344. In

348 the first part, the reactor temperature is set at 25°C and the pressure on the permeate side at 3mbar.
349 In the second part, the study is carried out at 40°C and the pressure is set at 8mbar.

350 **3.3.1. Experiments performed at 25°C**

351 At 25°C, all the experiments are performed with the M2 membrane in the following sequence: (1)
352 $w_{EtOH,ini}$ = 0.252, (2) $w_{EtOH,ini}$ = 0.344 and (3) $w_{EtOH,ini}$ = 0.122. The results are presented in Figure 9.

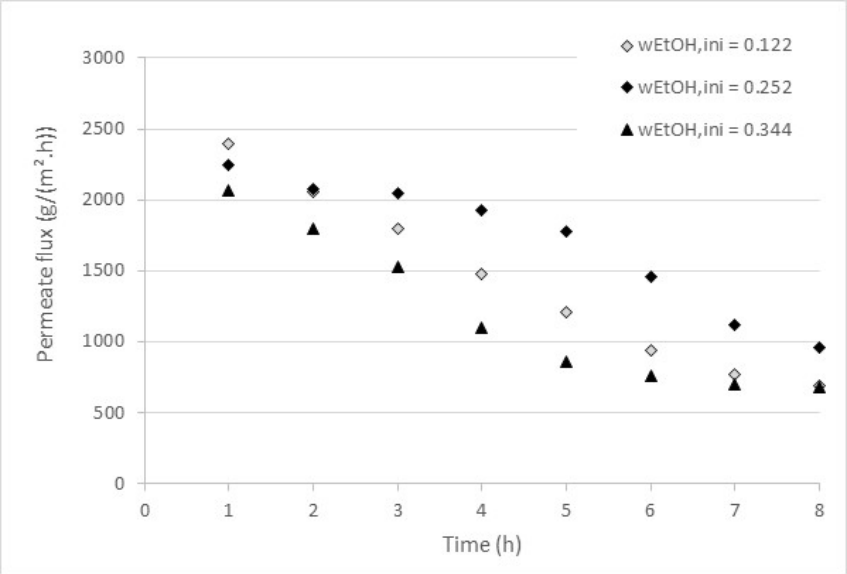


353

354 ***Figure 9.*** *Permeate flux as function of time for various initial ethanol mass fractions at T=25°C and*
355 *$P_{permeate}$ = 3mbar*

356 Whatever the initial ethanol mass fraction, the permeate flux decreases continuously during the
357 experiment. After 1h, the flux decreases from 2,395g/($m^2$.h) to 2,056g/($m^2$.h) for $w_{EtOH,ini}$ = 0.122; from
358 2,241g/($m^2$.h) to 2,079g/($m^2$.h) for $w_{EtOH,ini}$ = 0.252 and from 2,070g/($m^2$.h) to 1,798g/($m^2$.h) for
359 $w_{EtOH,ini}$ = 0.344. This flux decrease could be due to polarization concentration of ethanol and L-glu, but
360 also to the apparition of the first crystals in the reactor (confirmed by the *in situ* video), less than 2h
361 after the beginning of the experiment, those probably also be responsible in membrane fouling.
362 The permeate flux for $w_{EtOH,ini}$ = 0.252 is slightly higher than the other fluxes whereas the expected
363 result is a decrease of the permeate flux with the increase of the ethanol mass fraction. This is probably
364 because the membrane has been used first for $w_{EtOH,ini}$ = 0.344 and $w_{EtOH,ini}$ = 0.122.
365 Despite these results, the *in situ* observation, confirmed by OM and by XRD, highlights that the main
366 polymorphic form obtained is the $\alpha$-form.

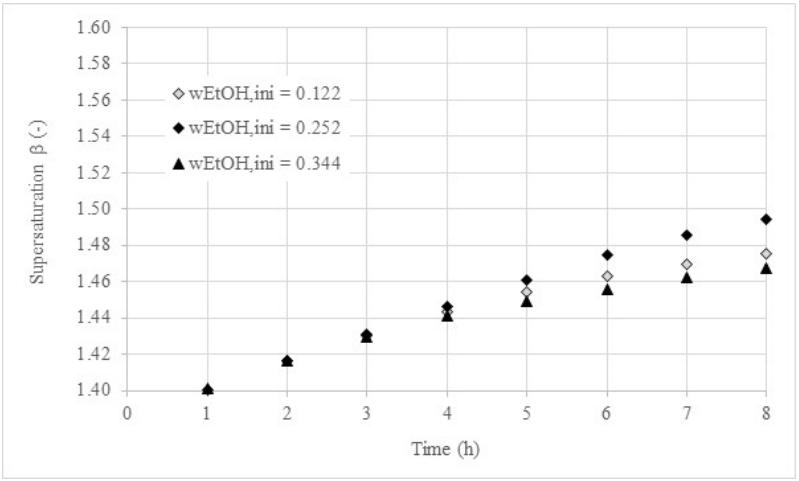


***Figure 10.*** *Supersaturation as a function of time for various initial ethanol mass fractions at T=25°C and* $P_{permeate}$ *= 3mbar*

Results reported in Figure 10 highlight that the supersaturation do not change a lot during the experiments whatever the composition of the feed solution. The supersaturation variation during the experiments are similar to the one reported on Figure 8 at 25°C being consistent with the observation of the preferential crystallization of the $\alpha$-form.

### 3.3.2. Experiments performed at 40°C

Results obtained at 40°C are reported on Figure 11. They show that, after 1h of experiment, the highest flux is reached for $w_{EtOH,ini}$ = 0.122, close to 4,703g/($m^2$.h) corresponding to twice the permeate flux for $w_{EtOH,ini}$ = 0.252 (2,690g/($m^2$.h)) and almost thrice for $w_{EtOH,ini}$ = 0.344 (1,420g/($m^2$.h)).

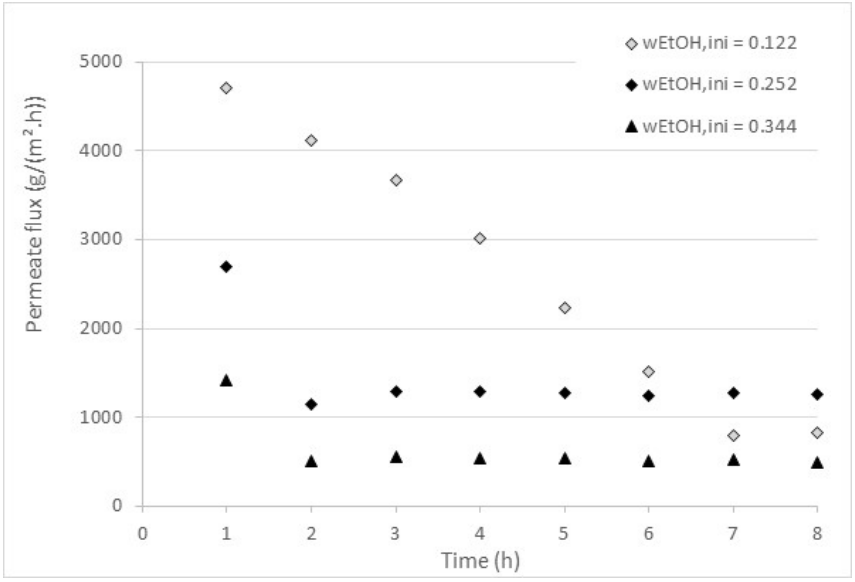


***Figure 11.*** *Permeate flux as function of time for various initial ethanol mass fractions at T=40°C and* $P_{permeate}$ *= 8mbar*

As reported previously, a significant decrease of the permeate flux is observed after 1 or 2h of experiment, especially for $w_{EtOH,ini}$ = 0.252 and $w_{EtOH,ini}$ = 0.344. The permeate fluxes then stabilize around 1,250g/($m^2$.h) and 500g/($m^2$.h), respectively. This may be the consequence of the formation of

a concentration polarization layer at the membrane surface. This phenomenon is well described for ultrafiltration and reverse osmosis processes [51]. Moreover, membrane fouling due to the accumulation of L-glu crystals and/or adsorption of L-glu molecules at the membrane surface can occur and induce a decrease in the permeate flux during the experiment [52]. Concentration polarization and/or fouling may be concomitant with the appearance of the first crystals, after the first hour of pervaporation, contributing more to this decrease.

***Table 6.*** *Polymorphic forms obtained at 40°C, $P_{permeate}$ = 8mbar*

| $w_{EtOH,initial}$ | **0.122** | **0.252** | **0.344** |
|---|---|---|---|
| **Membrane (number of use)** | M2 (5th use) | M2 (9th use) | M2 (10th use) |
| **Mean flux (g/(m².h))** | 2,606 | 1,431 | 636 |
| **OM Picture (enlargement x 5)*** | 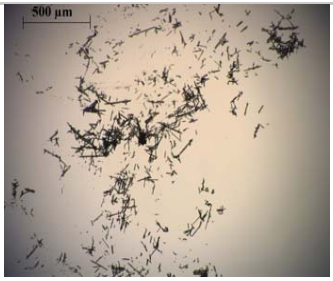  |  |  |
| **Polymorphic form obtained** | Mainly β<br>Fines needles | Mixture α + β<br>α: prismatic form<br>β: fines needles | Mainly β<br>Fines needles + sticks |

**OM pictures have the same scale: 500µm*

On the other hand, a more important decrease of the permeate flux is observed for $w_{EtOH,ini}$ = 0.122. In this case, the initial permeate flux is higher and the concentration polarization and/or fouling are slower. Nevertheless, after 8h of experiment, the permeate fluxes have similar values, whatever the initial ethanol mass fraction. Table 6 reports the mean fluxes during the experiments and the polymorphic forms obtained. The β-form is the main polymorphic form for $w_{EtOH,ini}$ = 0.122 and $w_{EtOH,ini}$ = 0.344 (cf. Table 6). Crystals look like fine needles with a rather heterogeneous size. However, for $w_{EtOH,ini}$ = 0.252, the α-form is mainly observed with a prismatic shape. These results are also confirmed by XRD.

The evolution of the supersaturation during experiments at 40°C are reported in Figure 12 and show that the supersaturation increases faster if the ethanol mass fraction in the feed solution is low. These results are consistent with the flux results reported on Figure 11 and with the formation of the concentration polarization layer at the membrane surface.

Figure 12 also confirms that whatever the supersaturation variation, the temperature seems to be the key parameter to control polymorphism.

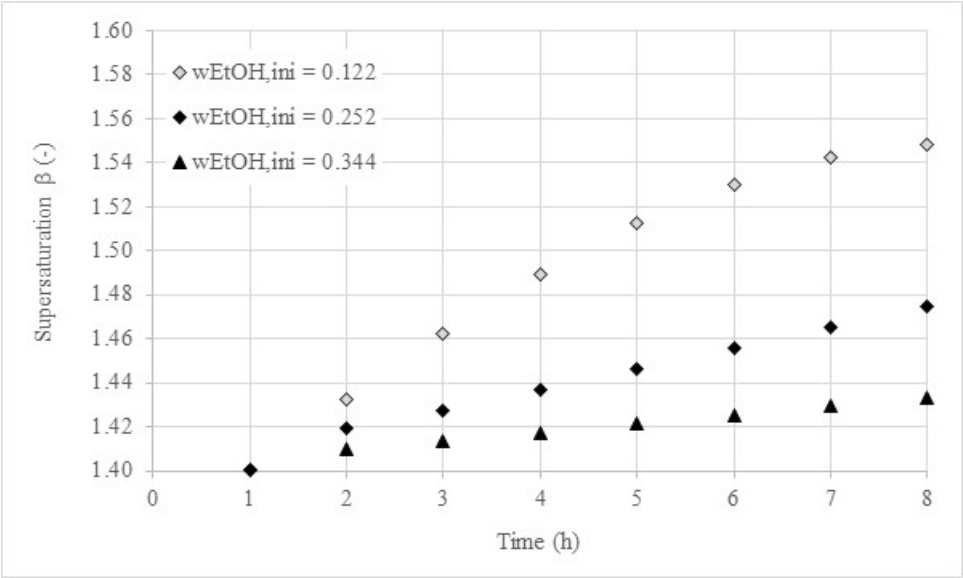


406

407 ***Figure 12.*** *Supersaturation as a function of time for various initial ethanol mass fractions at T=40°C and*
408 *$P_{permeate}$ = 8mbar*

409 ### *3.4. Influence of seeding*

410 The addition of crystal seeds of the metastable α-form is studied. The α-form is preferred in the
411 industry [10] and its addition as a seed should allow preferential production of this polymorphic form.
412 The seed is added at supersaturation (β = 1.4), 1h after the beginning of the experiment. The quantity
413 introduced corresponds to 5% of the expected theoretical final mass (cf. Table 1).
414 Seeding is expected to avoid heterogeneous nucleation by favouring the deposition of solute by growth
415 on the seed crystals rather than the production of new nuclei. Consequently, seeding allows an
416 increase in the size of the crystals and improves the polymorphism control [53,54].
417 In this part, the following operating parameters are fixed: T=25°C and $P_{permeate}$=3mbar. All experiments
418 with seeding are performed with the M1 membrane while experiments without seeding are performed
419 with the M2 membrane.
420 In addition, a test with β-seed is carried out at T=25°C for $w_{EtOH,ini}$ = 0.122. This is to confirm that the
421 control of the polymorphic phase can be achieved by seeding.

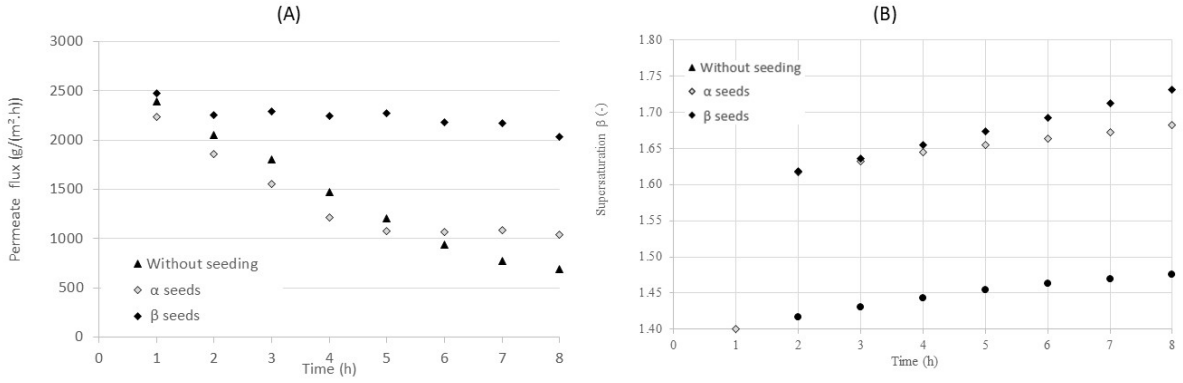


422

423 ***Figure 13.*** *Evolution of permeate fluxes (A) and supersaturation (B) with $\alpha$ or $\beta$ seeds and without*
424 *seeding for $w_{EtOH,ini}$ = 0.122, at 25°C and $P_{permeate}$ = 3mbar*

Figure 13 (A) shows that permeate fluxes of the experiments performed with α seeds and without seeding are close, whereas a higher and almost constant flux is achieved with the experiment seeded with β polymorph. Figure 13 (B) reports the evolution of the supersaturation during the experiment and confirms flux results: the supersaturation variation during the experiment (from 1 to 8h) is of the same order of magnitude without or with α seeding and is lower than with β seeds. Both experiments with seeding are performed with the M1 membrane: first the experiment with β seeds then with α seeds. The seed crystals are added to the solution 1h after the beginning of pervaporation. A difference is noticeable when comparing the experiments without and with β seeding since a higher and more stable flux is obtained for the experiment with β seeds. This may be due to the deposition of the L-glu by growth on the seed crystals rather than the production of new nuclei thus limiting the adsorption of L-glu on the membrane surface and hence its fouling. However, the addition of α seeds shows the lowest permeate flux. This difference could be due to the ageing of the membrane as reported previously.

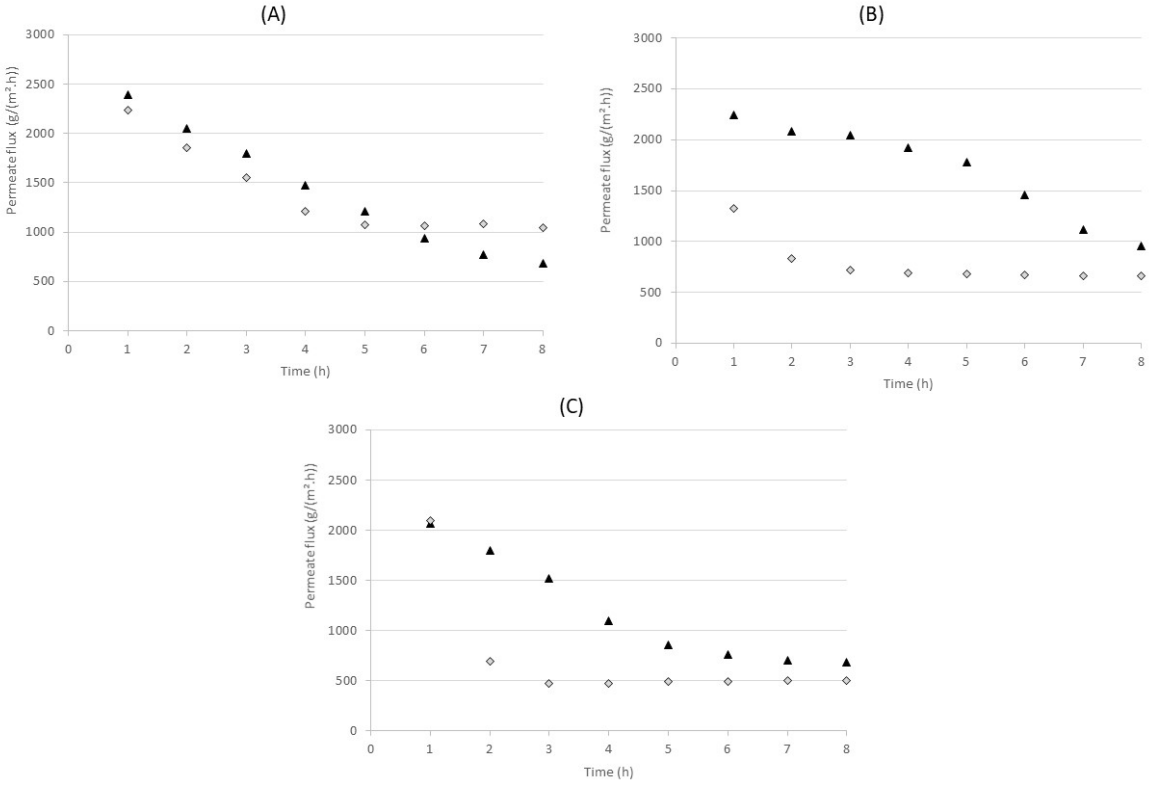


***Figure 14.*** *Evolution of permeate fluxes as a function of time with α seeds (◊) and without seeding (▲) for (A) $w_{EtOH,ini}$ = 0.122, (B) $w_{EtOH,ini}$ = 0.252, (C) $w_{EtOH,ini}$ = 0.344, at 25°C and $P_{permeate}$ = 3mbar*

The addition of β seeds provides mainly crystals of β-form with a rather heterogeneous size distribution, with fine needles and rod shapes (cf. Table 7). Seeding with crystals of α-form allows keeping the α-form preferentially obtained without seeding at the same operating conditions while increasing the size of the crystals (comparison of observations made under OM). These results are confirmed by XRD.

***Table 7.*** *Comparison of polymorphic forms obtained with or without seeding for $w_{EtOH,ini}$ = 0.122, at 25°C and $P_{permeate}$ = 8mbar*

| | No seeding | α seeds | β seeds |
|---|---|---|---|
| **Membrane (number of use)** | M2 (3rd use) | M1 (5th use) | M1 (4th use) |
| **OM Picture (enlargement x 5)*** | 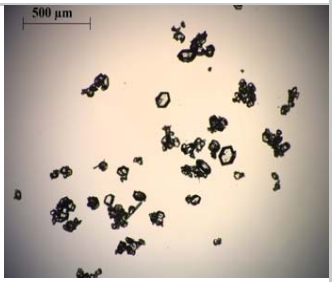  | 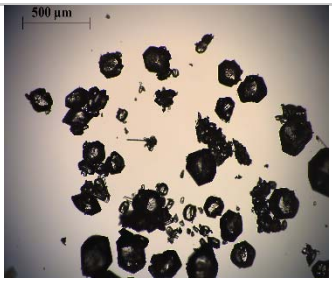  | 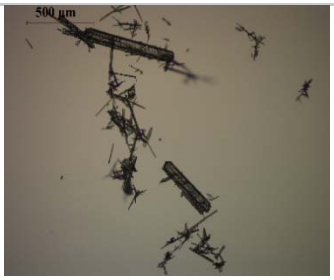  |
| **Polymorphic form obtained** | Mainly α | Mainly α | Mainly β |

**OM pictures have the same scale: 500µm*

The experiments are then carried out with α seeds or without seeding for several initial ethanol mass fractions. The results are presented in Figure 14 and show that the permeate flux decreases after the addition of the seed. However, this decrease is more important for $w_{EtOH,ini}$ = 0.252 and $w_{EtOH,ini}$ = 0.344. For $w_{EtOH,ini}$ = 0.122, the permeate fluxes with or without seeding are very close whereas a decrease is expected, as reported for the two other ethanol mass fractions. This phenomenon could be due to the membrane M2 aging for $w_{EtOH,ini}$ = 0.252 and $w_{EtOH,ini}$ = 0.344, i.e. with or without seeding; while two membranes (M1 and M2) are used which could explain the flux difference observed with the two other ethanol mass fractions.

The main results for each ethanol mass fraction with or without seeding are shown in Tables 7, 8 and 9.

***Table 8.*** *Comparison of polymorphic forms obtained with α seeds or without seeding for $w_{EtOH,ini}$ = 0.252, at 25°C and $P_{permeate}$ = 8mbar*

| | No seeding | Seeding |
|---|---|---|
| **Membrane (number of use)** | M2 (1st use) | M2 (6th use) |
| **OM Picture (enlargement x 5)*** |   | 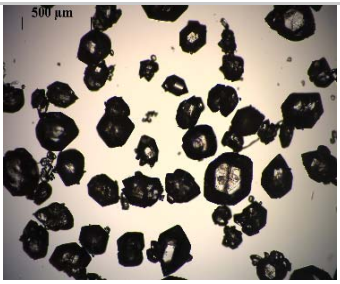  |
| **Polymorphic form obtained** | Mainly α | Mainly α |

**OM pictures have the same scale: 500µm*

***Table 9.*** *Comparison of polymorphic forms obtained with $\alpha$ seeds or without seeding for $w_{EtOH,ini}$ 0.344, at 25°C and $P_{permeate}$ = 8mbar*

| | No seeding | Seeding |
|---|---|---|
| **Membrane (number of use)** | M2 (2nd use) | M2 (7th use) |
| **OM Picture (enlargement x 5)*** | Not enough of crystals |  |
| **Polymorphic form obtained** | / | Mainly α |

**OM pictures have the same scale: 500µm*

As shown in Table 7 to Table 9, the metastable form is mainly obtained at 25°C whatever the ethanol mass fraction, with or without seeding. A significant increase in crystal size is observed after seeding. On the other hand, in the experiments achieved with seeding, traces of β-form are detected by the *in situ* video probe and some crystals are observed under OM. These results are also confirmed by XRD.

# 4. DISCUSSION

The permeate flux variations over time and after several uses, the adsorption of L-glu on the membrane surface and the influence of the operating parameters on the polymorphic forms obtained are successively discussed below.

## *4.1. Change of the permeate flux*

During the first use of the HybSi® membrane for crystallization using pervaporation, the permeate flux remains constant over 8h, with only a slight decrease of the flux with time, except in the case of the M2 membrane (cf. Figure 4). Indeed, important decrease of the permeate flux with time is observed after the first use. Similar decrease in permeate flux is reported in the literature for the organic solvent dehydration by pervaporation [43,46]. Nevertheless, the decrease reported is not as important and it is difficult to compare it to our results, where pervaporation is associated to crystallization.

During pervaporation of water/ethanol solutions, the permeate flux is almost constant during 5h, whatever the ethanol mass fraction studied. This observation means that ethanol is not the main responsible for the decrease observed in our pervaporation/crystallization experiments. Hence, L-glu seems to have a direct influence on the observed permeate flux decrease.

Therefore, the adsorption of L-glu and the formation of crystals at the membrane surface could be responsible for the progressive decrease of water permeation through the membrane (cf. Figure 15). Thus, it is assumed that a series of events, as described below, contributes to this phenomenon:

i. The preferential diffusion of water through the hydrophilic membrane contributes to create a concentration polarization layer of ethanol and dissolved L-glu at the membrane surface. The formation of this boundary layer could explain the stable permeate flux after 1 or 2h, according to the experimental conditions.

ii. The tangential flow does not provide sufficient shear stress to "sweep" the accumulated molecules and/or crystals along the membrane surface, even under turbulent conditions.

iii. In parallel, the crystals' formation near and at the membrane surface, which is the place where the supersaturation is the most important, contributes to decrease the permeate flux with time by adding a surface fouling phenomenon. In addition, the evaporation of water through the membrane produces a local cooling leading to faster crystallization at the surface and near the membrane.

When these phenomena are not reversible, the membrane regeneration is not sufficient to restore the initial flux and the membrane performance decreases with the number of uses.

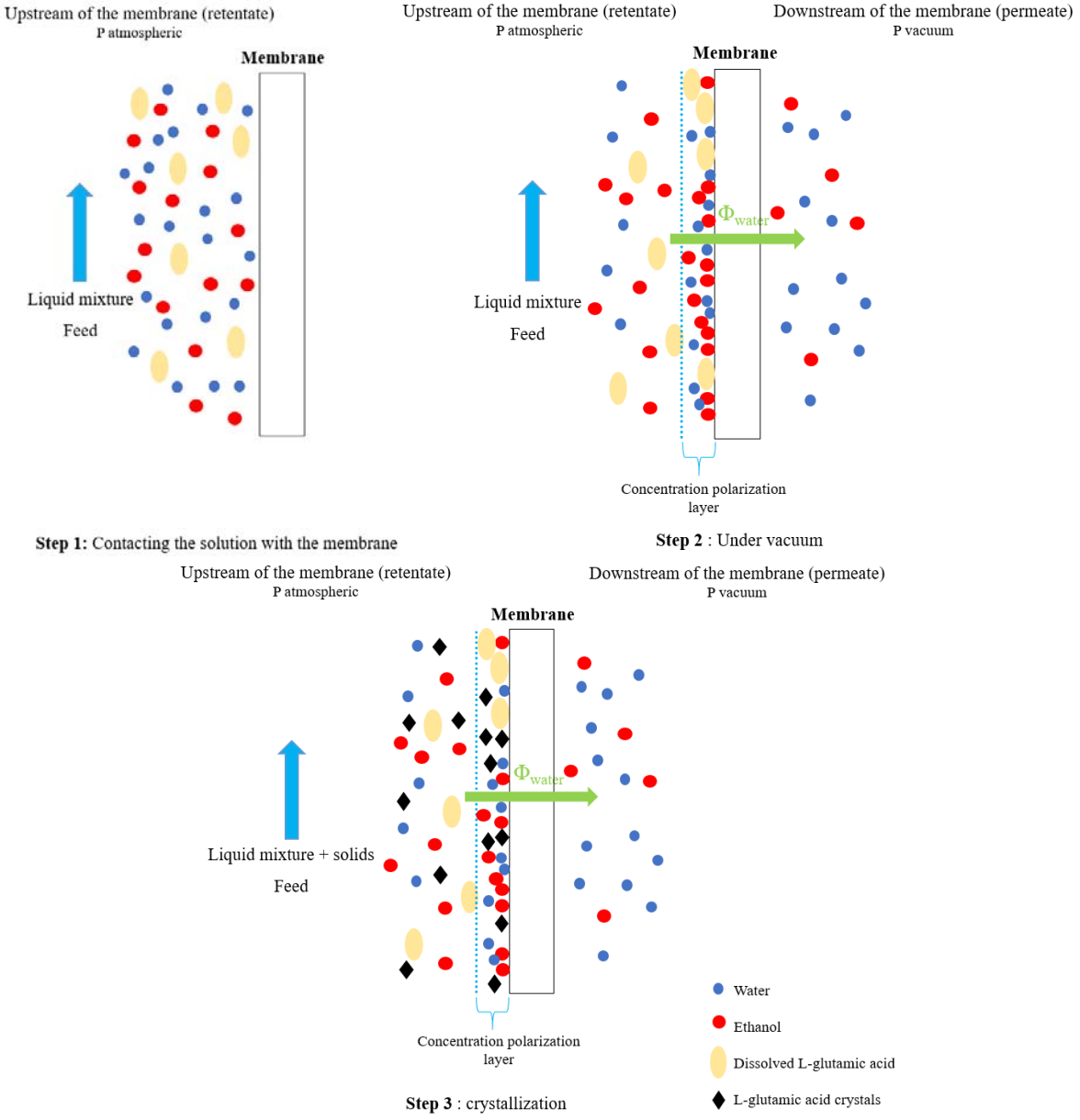


***Figure 15.*** *Illustration of concentration polarization and fouling during crystallization using pervaporation*

### *4.2. Adsorption of L-glutamic acid at the HybSi® membrane surface*

As reported in the seeding part, a decrease in the permeate flux is observed with time during the experiments but also with repeated uses of the HybSi® membrane. The adsorption of L-glu at the membrane surface could be an explanation for the fouling phenomenon.

L-glu is available under several chemical forms according to the pH of the solution: a cationic form at pH ≤ 2.19, an anionic form at pH ≥ 4.25, and a zwitterionic form between 2.19 and 4.25 [55].

In addition, BTESM is a precursor belonging to the organoalkoxysilane family. According to the position of the organic groups ($CH_2$ and $CH_3$) in the organosilica networks, BTSEM has two configurations: (1) the bridging position type (-Si-$CH_2$-Si-), (2) the terminal position (-Si-$CH_3$) [56]. Both types are reported in Figure 16. Organic groups are much considered as spacers between silica atoms of the structure of the organosilica networks. If the organic groups are in a terminal position, they don't act like spacers and can easily fill the pores created by the silica structure as shown in Figure 16 [42,57].

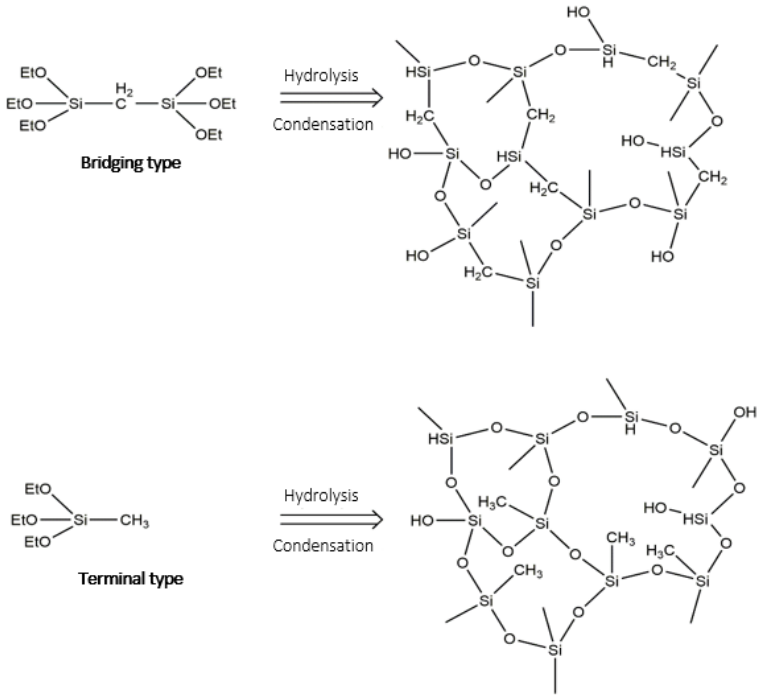


***Figure 16.*** *Possible configuration of BTESM: bridging and terminal position and their derived networks* [56]

There are free -OH groups on the surface of the membrane, responsible for its hydrophilic nature. These groups are also able to interact with L-glu molecules by making hydrogen bonds with the –COOH groups. This phenomenon has been previously described for the dehydration of ethyl acrylate from acrylic acid using a PVA membrane [49]. The stability study of these membranes has been performed by comparing results obtained on a new membrane and an artificially aged membrane. The analysis, achieved by IR spectroscopy, showed changes after one month of continuous pervaporation. The –OH groups decreased while a significant increase in the C=O groups have been detected. The authors assumed that it could be due to a chemical reaction between the –OH group of the membrane and acrylic acid [49].

Hence, adsorption of L-glu molecules on the membrane surface can lead to a significant decrease in the permeate flux during the experiment. Moreover, the dissolved L-glu molecules can promote heterogeneous nucleation at the membrane surface, as the solution is locally highly supersaturated. These nuclei could also extend on the membrane surface and thus contribute to a further decrease in the flux. Hence, a decrease of the membrane performance, due to degradation of the selective fine layer of HybSi®, is expected after a certain number of use (after around 12 uses for the M2 membrane, fluxes and separation factors have been divided by 2 (data not shown)).

### *4.3. Influence of operating parameter on the polymorphic form obtained*

Table 10 summarize the polymorphic forms obtained according to the operating conditions for two ethanol mass fractions.

***Table 10.*** *Summary of the polymorphic forms obtained for $w_{EtOH,ini}$ = 0.122*

| Operating parameter | | Polymorphic form |
|---|---|---|
| **Permeate pressure (mbar)** | 3 | Mainly α |
| | 8 | Mainly α |
| **Temperature (°C)** | 25 | Mainly α |
| | 40 | Mainly β |
| **Seeding at 25°C** | - | Mainly α |
| | α | Mainly α |
| | β | Mainly β |
| **Seeding at 40°C** | - | Mainly β |
| | α | Mixture of α and β but mainly β |

Table 10 highlights that temperature has a significant influence on the selection of the polymorphic form for the ethanol mass fraction of 0.122. Indeed, the $\alpha$-form is the main polymorphic form produced at 25°C while it is the $\beta$-form at 40°C. However, the increase of the permeate pressure does not influence the polymorphic form for $w_{EtOH,ini}$ = 0.122 (cf. Table 10).

In contrast, a mixture of both polymorphs, mainly with the $\alpha$-form is observed at 40°C for $w_{EtOH,ini}$ = 0.252, (cf. Table 11). At the beginning of the experiment, the α-form is observed and then a phase transition occurs. At high temperatures, the thermodynamically stable β-form tends to crystallize preferentially.

***Table 11.*** *Summary of the polymorphic forms obtained for $w_{EtOH,ini}$ = 0.252, at $P_{permeate}$ = 3mbar*

| Operating parameters | | Polymorphic form obtained |
|---|---|---|
| **Seeding at 25°C** | - | Mainly α |
| | α | Mainly α |
| **Seeding at 40°C** | - | Mixture of α and β but mainly α |
| | α | Mixture of α and β but mainly α |

These observations are consistent with those reported in the literature [58,59]. Indeed, one of the key parameters to control the crystallization of a polymorphic form on another seems to be the temperature. According to the work of Tahri et al., at low temperature (≈ 5°C) and low supersaturation,

the nucleation and growth of polymorph α are faster and a preferential crystallization of this polymorph is observed [60]. In this work, metastable crystals are spontaneously obtained at 25°C for $w_{EtOH,ini}$ = 0.122 and $w_{EtOH,ini}$ = 0.252, and at 40°C for $w_{EtOH,ini}$ = 0.252. The addition of antisolvent in the initial solution moves the nucleation area of the α-form forward. This behaviour follows the Ostwald rules of stages which suggests that a chemical system does not tend the most stable state, but rather tends towards the closest metastable state [61].

Tahri et al. suggested a kinetic explanation of the Oswald rules of stages, based on an original ripening mechanism occurring between polymorphs clusters [60]. According to the authors, in the first step of the crystallization, at the nanometric scale, both polymorphs nucleate. Nevertheless, because of the rapid growth of the metastable phase clusters consuming the supersaturation, the slow-growing clusters of the stable polymorph become undersaturated and dissolve (cf. Figure 17). Therefore, if the difference in growth kinetics between the polymorphs is high while their equilibrium concentrations are close, the Gibbs-Thomson effect may allow the preferential crystallization of the metastable polymorph at the expense of the stable polymorph, leading to the macroscopic observation of Ostwald rules of stages [60].

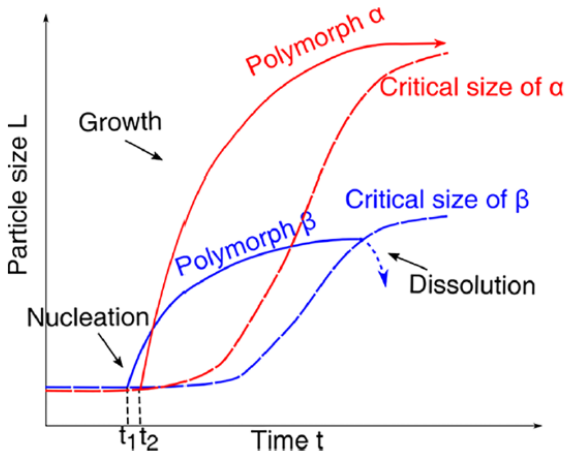


***Figure 17.*** *Competition between both polymorphs of L-glutamic acid, leading to the production of the metastable α polymorph [60]*

At high temperatures (≥ 40°C) and low supersaturation, the nucleation rate of the α-form is low while the growth rate of the β-form is more important. In the competition between the two polymorphs, β nuclei sizes manage then to remain over the critical size all along the nucleation process which justifies the prevalence of the β-form [62].

Of all the different parameters involved in the crystallization process of polymorphs, the suggested ripening mechanism seems to have an important role. Considering this mechanism between polymorphs could be useful for the control of the polymorphic phase obtained in industrial processes or for their screening.

## 5. CONCLUSION

This study describes the pervaporation process applied to the crystallization of L-glu. The purpose is to determine the experimental parameters allowing the control of the crystals' final properties (size and polymorphic form) and to identify the limiting parameters of the process. It is found that temperature

is a major parameter that controls the membrane's selectivity as well as the polymorphic phases produced. Moreover, a significant decrease in permeate flux as a function of time is obtained for experimental conditions where the initial flux is high. Stabilization of the flux after 1h or 2h of pervaporation is observed, for lower initial flux values. The permeate flux also decreases with the repeated use of the same membrane, the regeneration does not allow to find the initial value of the flux. The achievement of a stabilized flux after 1h or 2h of pervaporation/crystallization can be explained by the formation of a boundary layer on the surface of the membrane. The decrease in permeate flux is the consequence of several phenomena: the concentration polarization of ethanol and L-glu acid molecules and membrane fouling as result of the adsorption of dissolved L-glu acid molecules and L-glu crystallization on the membrane surface (where supersaturation is locally very high). Fouling contributes after several uses, to reduce the performance of the membrane and therefore the process.

Results obtained show the feasibility of the pervaporation process applied to the crystallization of L-glu. It is found that the polymorph formed does not directly depend on the permeate flux but more on the operating conditions and particularly on the temperature and the mass fraction of ethanol in the initial water/ethanol mixture.

## LIST OF SYMBOLS AND ABBREVIATIONS

### *Abbreviations*

BTESE: bis(triethoxysilyl)ethane
BTESM: bis(triethoxysilyl)methane
CSD: Crystal Size Distribution
$D_2O$: Deuterium oxide
M1, M2, M3: membrane 1, 2, 3
NMR: Nuclear Magnetic Resonance
OM: Optical Microscopy
SEM: Scanning Electron Microscopy
STP: Sodium 3-trimethylsilyl-3,3,2,2-tetradeuteriopropionate
XRD: X-Ray Diffraction

### *Symbols*

α: Metastable polymorph of L-glutamic acid
β: Stable polymorph of L-glutamic acid
$\beta_{water/EtOH}$: water/ethanol separation factor (-)
$J_i$: Partial flux of compound i (kg/($m^2$.h))
$J_{tot}$: Total flux of permeate (kg/($m^2$.h))
$m_p$: Mass of permeate recovered in the trap (g)
Re: Reynolds number
S: Effective membrane area ($m^2$)
t: Time (h)
$w_i^p$: Mass fraction of compound i in the permeate (-)

### *Index and exposits*

EtOH : Ethanol

f: feed
i: Chemical species considered (water or ethanol)
ini: Initial
L-glu : Acide L-glutamique
p : Permeate
tot : Total
w : Water

## ACKNOWLEDGEMENTS

We would like to thank Ruben Vera for the X-ray diffraction measurements (Centre de Diffractométrie Henri Longchambon, Université Lyon 1, Villeurbanne - France) and Emmanuel Chefdeville for the NMR analysis (Centre Commun de RMN, Université Lyon 1, Villeurbanne - France).

## BIBLIOGRAPHY

[1] B.Y. Shekunov, P. York, Crystallization processes in pharmaceutical technology and drug delivery design, Journal of Crystal Growth. 211 (2000) 122–136. https://doi.org/10.1016/S0022-0248(99)00819-2.

[2] T.-T.C. Lai, S. Ferguson, L. Palmer, B.L. Trout, A.S. Myerson, Continuous Crystallization and Polymorph Dynamics in the L -Glutamic Acid System, Org. Process Res. Dev. 18 (2014) 1382–1390. https://doi.org/10.1021/op500171n.

[3] J. Orehek, D. Teslić, B. Likozar, Continuous Crystallization Processes in Pharmaceutical Manufacturing: A Review, Org. Process Res. Dev. 25 (2021) 16–42. https://doi.org/10.1021/acs.oprd.0c00398.

[4] M. Michaud, D. Mangin, C. Charcosset, E. Chabanon, Dense Membrane Crystallization in Gas–Liquid Systems: Key Parameters Influencing Fouling, Ind. Eng. Chem. Res. 58 (2019) 20134–20146. https://doi.org/10.1021/acs.iecr.9b03907.

[5] C. Charcosset, Membrane processes in biotechnology: An overview, Biotechnology Advances. 24 (2006) 482–492. https://doi.org/10.1016/j.biotechadv.2006.03.002.

[6] C. Charcosset, R. Kieffer, D. Mangin, F. Puel, Coupling between Membrane Processes and Crystallization Operations, Industrial & Engineering Chemistry Research. 49 (2010) 5489–5495. https://doi.org/10.1021/ie901824x.

[7] E. Drioli, G. Di Profio, E. Curcio, Progress in membrane crystallization, Current Opinion in Chemical Engineering. 1 (2012) 178–182. https://doi.org/10.1016/j.coche.2012.03.005.

[8] G. Di Profio, S. Tucci, E. Curcio, E. Drioli, Controlling Polymorphism with Membrane-Based Crystallizers: Application to Form I and II of Paracetamol, Chemistry of Materials. 19 (2007) 2386–2388. https://doi.org/10.1021/cm0701005.

[9] G. Di Profio, S. Tucci, E. Curcio, E. Drioli, Selective Glycine Polymorph Crystallization by Using Microporous Membranes, Crystal Growth & Design. 7 (2007) 526–530. https://doi.org/10.1021/cg0605990.

[10] G. Di Profio, E. Curcio, S. Ferraro, C. Stabile, E. Drioli, Effect of Supersaturation Control and Heterogeneous Nucleation on Porous Membrane Surfaces in the Crystallization of L-Glutamic Acid Polymorphs, Crystal Growth & Design. 9 (2009) 2179–2186. https://doi.org/10.1021/cg800838b.

[11] G. Di Profio, C. Stabile, A. Caridi, E. Curcio, E. Drioli, Antisolvent membrane crystallization of pharmaceutical compounds, Journal of Pharmaceutical Sciences. 98 (2009) 4902–4913. https://doi.org/10.1002/jps.21785.
[12] G. Di Profio, M.T. Reijonen, R. Caliandro, A. Guagliardi, E. Curcio, E. Drioli, Insights into the polymorphism of glycine: membrane crystallization in an electric field, Physical Chemistry Chemical Physics. 15 (2013) 9271. https://doi.org/10.1039/c3cp50664a.
[13] E. Drioli, G. Di Profio, E. Curcio, Membrane-assisted crystallization technology, World Scientific, London ; Hackensack, NJ, 2015.
[14] G. Di Profio, V. Grosso, A. Caridi, R. Caliandro, A. Guagliardi, G. Chita, E. Curcio, E. Drioli, Direct production of carbamazepine–saccharin cocrystals from water/ethanol solvent mixtures by membrane-based crystallization technology, CrystEngComm. 13 (2011) 5670. https://doi.org/10.1039/c1ce05410d.
[15] A. Jonquières, R. Clément, P. Lochon, J. Néel, M. Dresch, B. Chrétien, Industrial state-of-the-art of pervaporation and vapour permeation in the western countries, Journal of Membrane Science. 206 (2002) 87–117. https://doi.org/10.1016/S0376-7388(01)00768-2.
[16] C.S. Slater, M.J. Savelski, T.M. Moroz, M.J. Raymond, Pervaporation as a green drying process for tetrahydrofuran recovery in pharmaceutical synthesis, Green Chemistry Letters and Reviews. 5 (2012) 55–64. https://doi.org/10.1080/17518253.2011.578590.
[17] D. Shah, K. Kissick, A. Ghorpade, R. Hannah, D. Bhattacharyya, Pervaporation of alcohol–water and dimethylformamide–water mixtures using hydrophilic zeolite NaA membranes: mechanisms and experimental results, Journal of Membrane Science. 179 (2000) 185–205. https://doi.org/10.1016/S0376-7388(00)00515-9.
[18] C. Yu, Y. Liu, G. Chen, X. Gu, W. Xing, Pretreatment of Isopropanol Solution from Pharmaceutical Industry and Pervaporation Dehydration by NaA Zeolite Membranes, Chinese Journal of Chemical Engineering. 19 (2011) 904–910. https://doi.org/10.1016/S1004-9541(11)60071-2.
[19] D. Shah, D. Bhattacharyya, A. Ghorpade, W. Mangum, Pervaporation of pharmaceutical waste streams and synthetic mixtures using water selective membranes, Environmental Progress. 18 (1999) 21–29. https://doi.org/10.1002/ep.670180116.
[20] R.W. Baker, Membrane technology and applications, 2nd ed, J. Wiley, Chichester ; New York, 2004.
[21] G. Liu, W. Jin, Pervaporation membrane materials: Recent trends and perspectives, Journal of Membrane Science. 636 (2021) 119557. https://doi.org/10.1016/j.memsci.2021.119557.
[22] X. Cheng, F. Pan, M. Wang, W. Li, Y. Song, G. Liu, H. Yang, B. Gao, H. Wu, Z. Jiang, Hybrid membranes for pervaporation separations, Journal of Membrane Science. 541 (2017) 329–346. https://doi.org/10.1016/j.memsci.2017.07.009.
[23] P.A. Kober, Pervaporation, Persitallation and Percrystallization, J. Am. Chem. Soc. 39 (1917) 944–948. https://doi.org/10.1021/ja02250a011.
[24] K.W. Böddeker, I.L. Gatfield, J. Jähnig, C. Schorm, Pervaporation at the vapor pressure limit: Vanillin, Journal of Membrane Science. 137 (1997) 155–158. https://doi.org/10.1016/S0376-7388(97)00187-7.
[25] X. Zhang, C. Li, X. Hao, X. Feng, H. Zhang, H. Hou, G. Liang, Recovering phenol as high purity crystals from dilute aqueous solutions by pervaporation, Chemical Engineering Science. 108 (2014) 183–187. https://doi.org/10.1016/j.ces.2014.01.011.
[26] C. Li, X. Zhang, X. Hao, X. Feng, X. Pang, H. Zhang, Thermodynamic and mechanistic studies on recovering phenol crystals from dilute aqueous solutions using pervaporation–crystallization coupling (PVCC) system, Chemical Engineering Science. 127 (2015) 106–114. https://doi.org/10.1016/j.ces.2015.01.039.
[27] W. Zeng, B. Li, H. Li, H. Jin, D. Wu, Y. Li, A pervaporation-crystallization (PC) process for simultaneous recovery of ethanol and sodium pyruvate from waste centrifugal mother liquid, Journal of Membrane Science. 619 (2021) 118749. https://doi.org/10.1016/j.memsci.2020.118749.

[28] M. Gryta, Fouling in direct contact membrane distillation process, Journal of Membrane Science. 325 (2008) 383–394. https://doi.org/10.1016/j.memsci.2008.08.001.
[29] R. Kieffer, D. Mangin, F. Puel, C. Charcosset, Precipitation of barium sulphate in a hollow fiber membrane contactor, Part I: Investigation of particulate fouling, Chemical Engineering Science. 64 (2009) 1759–1767. https://doi.org/10.1016/j.ces.2009.01.011.
[30] X. Zhang, L. Fan, F.A. Roddick, Effect of feedwater pre-treatment using UV/H2O2 for mitigating the fouling of a ceramic MF membrane caused by soluble algal organic matter, Journal of Membrane Science. 493 (2015) 683–689. https://doi.org/10.1016/j.memsci.2015.07.024.
[31] B. Ma, W. Xue, Y. Bai, R. Liu, W. Chen, H. Liu, J. Qu, Enhanced alleviation of ultrafiltration membrane fouling by regulating cake layer thickness with pre-coagulation during drinking water treatment, Journal of Membrane Science. 596 (2020) 117732. https://doi.org/10.1016/j.memsci.2019.117732.
[32] R. Fabris, E.K. Lee, C.W.K. Chow, V. Chen, M. Drikas, Pre-treatments to reduce fouling of low pressure micro-filtration (MF) membranes, Journal of Membrane Science. 289 (2007) 231–240. https://doi.org/10.1016/j.memsci.2006.12.003.
[33] L.L.A. Koh, H.T.H. Nguyen, J. Chandrapala, B. Zisu, M. Ashokkumar, S.E. Kentish, The use of ultrasonic feed pre-treatment to reduce membrane fouling in whey ultrafiltration, Journal of Membrane Science. 453 (2014) 230–239. https://doi.org/10.1016/j.memsci.2013.11.006.
[34] A.S. Al-Amoudi, Factors affecting natural organic matter (NOM) and scaling fouling in NF membranes: A review, Desalination. 259 (2010) 1–10. https://doi.org/10.1016/j.desal.2010.04.003.
[35] E. Gwon, M. Yu, H. Oh, Y. Ylee, Fouling characteristics of NF and RO operated for removal of dissolved matter from groundwater, Water Research. 37 (2003) 2989–2997. https://doi.org/10.1016/S0043-1354(02)00563-8.
[36] R. Sheikholeslami, S. Zhou, Performance of RO membranes in silica bearing waters, Desalination. 132 (2000) 337–344. https://doi.org/10.1016/S0011-9164(00)00169-7.
[37] Y. Zhou, J. Wang, T. Wang, N. Wang, Y. Xiao, S. Zong, X. Huang, H. Hao, Self-Assembly of Monodispersed Carnosine Spherical Crystals in a Reverse Antisolvent Crystallization Process, Crystal Growth & Design. 19 (2019) 2695–2705. https://doi.org/10.1021/acs.cgd.8b01818.
[38] L. Martínez-Díez, M.I. Vázquez-Gonzàlez, Temperature polarization in mass transport through hydrophobic porous membranes, AIChE J. 42 (1996) 1844–1852. https://doi.org/10.1002/aic.690420706.
[39] I.L. Borisov, A. Kujawska, K. Knozowska, V.V. Volkov, W. Kujawski, Influence of feed flow rate, temperature and feed concentration on concentration polarization effects during separation of water-methyl acetate solutions with high permeable hydrophobic pervaporation PDMS membrane, Journal of Membrane Science. 564 (2018) 1–9. https://doi.org/10.1016/j.memsci.2018.07.001.
[40] B. Ravindra Babu, N.K. Rastogi, K.S.M.S. Raghavarao, Concentration and temperature polarization effects during osmotic membrane distillation, Journal of Membrane Science. 322 (2008) 146–153. https://doi.org/10.1016/j.memsci.2008.05.041.
[41] H.L. Castricum, R. Kreiter, H.M. van Veen, D.H.A. Blank, J.F. Vente, J.E. ten Elshof, High-performance hybrid pervaporation membranes with superior hydrothermal and acid stability, Journal of Membrane Science. 324 (2008) 111–118. https://doi.org/10.1016/j.memsci.2008.07.014.
[42] H.L. Castricum, G.G. Paradis, M.C. Mittelmeijer-Hazeleger, R. Kreiter, J.F. Vente, J.E. ten Elshof, Tailoring the Separation Behavior of Hybrid Organosilica Membranes by Adjusting the Structure of the Organic Bridging Group, Advanced Functional Materials. 21 (2011) 2319–2329. https://doi.org/10.1002/adfm.201002361.
[43] H.M. van Veen, M.D.A. Rietkerk, D.P. Shanahan, M.M.A. van Tuel, R. Kreiter, H.L. Castricum, J.E. ten Elshof, J.F. Vente, Pushing membrane stability boundaries with HybSi® pervaporation membranes, Journal of Membrane Science. 380 (2011) 124–131. https://doi.org/10.1016/j.memsci.2011.06.040.

[44] G.G. Paradis, D.P. Shanahan, R. Kreiter, H.M. van Veen, H.L. Castricum, A. Nijmeijer, J.F. Vente, From hydrophilic to hydrophobic HybSi® membranes: A change of affinity and applicability, Journal of Membrane Science. 428 (2013) 157–162. https://doi.org/10.1016/j.memsci.2012.10.006.
[45] M. Khellaf, C. Charcosset, D. Mangin, E. Chabanon, Solubility of L-glutamic acid in concentrated water/ethanol solutions, Journal of Crystal Growth. 570 (2021) 126238. https://doi.org/10.1016/j.jcrysgro.2021.126238.
[46] S.-K. Mah, S.-P. Chai, T.Y. Wu, Dehydration of glycerin solution using pervaporation: HybSi and polydimethylsiloxane membranes, Journal of Membrane Science. 450 (2014) 440–446. https://doi.org/10.1016/j.memsci.2013.09.048.
[47] E. Gagnière, D. Mangin, F. Puel, A. Rivoire, O. Monnier, E. Garcia, J.P. Klein, Formation of co-crystals: Kinetic and thermodynamic aspects, Journal of Crystal Growth. 311 (2009) 2689–2695. https://doi.org/10.1016/j.jcrysgro.2009.02.040.
[48] G. del Campo, J. Zuriarrain, A. Zuriarrain, I. Berregi, Quantitative determination of carboxylic acids, amino acids, carbohydrates, ethanol and hydroxymethylfurfural in honey by 1H NMR, Food Chemistry. 196 (2016) 1031–1039. https://doi.org/10.1016/j.foodchem.2015.10.036.
[49] H.T. Truong, S. Rode, D. Roizard, S. Mouzon-Pelletier, S. Tretjak, Dehydration of reactive industrial mixtures by pervaporation: An innovative approach in acrylic esters processes, Separation and Purification Technology. 120 (2013) 24–34. https://doi.org/10.1016/j.seppur.2013.09.017.
[50] A.V. Klinov, R.R. Akberov, A.R. Fazlyev, M.I. Farakhov, Experimental investigation and modeling through using the solution-diffusion concept of pervaporation dehydration of ethanol and isopropanol by ceramic membranes HybSi, Journal of Membrane Science. 524 (2017) 321–333. https://doi.org/10.1016/j.memsci.2016.11.057.
[51] S. Sablani, M. Goosen, R. Al-Belushi, M. Wilf, Concentration polarization in ultrafiltration and reverse osmosis: a critical review, Desalination. 141 (2001) 269–289. https://doi.org/10.1016/S0011-9164(01)85005-0.
[52] A. Giacobbo, A. Moura Bernardes, M.J. Filipe Rosa, M.N. De Pinho, Concentration Polarization in Ultrafiltration/Nanofiltration for the Recovery of Polyphenols from Winery Wastewaters, Membranes. 8 (2018) 46. https://doi.org/10.3390/membranes8030046.
[53] F. Zhang, B. Shan, Y. Wang, Z. Zhu, Z.-Q. Yu, C.Y. Ma, Progress and Opportunities for Utilizing Seeding Techniques in Crystallization Processes, Org. Process Res. Dev. 25 (2021) 1496–1511. https://doi.org/10.1021/acs.oprd.1c00103.
[54] Y. He, Z. Gao, T. Zhang, J. Sun, Y. Ma, N. Tian, J. Gong, Seeding Techniques and Optimization of Solution Crystallization Processes, Org. Process Res. Dev. 24 (2020) 1839–1849. https://doi.org/10.1021/acs.oprd.0c00151.
[55] M. Voges, I.V. Prikhodko, S. Prill, M. Hübner, G. Sadowski, C. Held, Influence of pH Value and Ionic Liquids on the Solubility of L-Alanine and L-Glutamic Acid in Aqueous Solutions at 30 °C, J. Chem. Eng. Data. 62 (2017) 52–61. https://doi.org/10.1021/acs.jced.6b00367.
[56] H. Zhang, D. He, S. Niu, H. Qi, Tuning the microstructure of organosilica membranes with improved gas permselectivity via the co-polymerization of 1,2-bis(triethoxysilyl)ethane and 1,2-bis(triethoxysilyl)methane, International Journal of Hydrogen Energy. 46 (2021) 17221–17230. https://doi.org/10.1016/j.ijhydene.2021.02.139.
[57] A.P. Dral, J.E. ten Elshof, Organic groups influencing microporosity in organosilicas, Microporous and Mesoporous Materials. 267 (2018) 267–273. https://doi.org/10.1016/j.micromeso.2018.03.036.
[58] J. Schöll, D. Bonalumi, L. Vicum, M. Mazzotti, M. Müller, In Situ Monitoring and Modeling of the Solvent-Mediated Polymorphic Transformation of L-Glutamic Acid, Crystal Growth & Design. 6 (2006) 881–891. https://doi.org/10.1021/cg0503402.
[59] Y. Tahri, E. Gagnière, E. Chabanon, T. Bounahmidi, D. Mangin, Investigation of the l-Glutamic acid polymorphism: Comparison between stirred and stagnant conditions, Journal of Crystal Growth. 435 (2016) 98–104. https://doi.org/10.1016/j.jcrysgro.2015.11.019.

[60] Y. Tahri, E. Gagnier, N. Candoni, Multiscale Experimental Study and Modeling of L-Glutamic acid Crystallization: Emphasis on a Kinetic Explanation of the Ostwald Rule of Stages, Cryst. Growth Des. (2019) 9.
[61] W. Ostwald, Studien über die Bildung und Umwandlung fester Körper: 1. Abhandlung: Übersättigung und Überkaltung, Zeitschrift für Physikalische Chemie. 22U (1897) 289–330. https://doi.org/10.1515/zpch-1897-2233.
[62] Y. Tahri, D. Mangin, Modeling the Competition between Polymorphic Phases: Highlights on the Effect of Ostwald Ripening, Cryst. Growth Des. (2016) 9.